Electronic supplementary materials *Mendeleev Commun.*, 2021, **31**, 532–535

Effect of spin polarization and supercell size on specific energy and electronic structure of MoS_2 edge calculated by DFT method in the plane-wave basis

Eugenii A. Permyakov, Vladimir V. Maximov and Victor M. Kogan

Calculation methodology

This study used the density functional method[S1] with the PBE functional[S2] in the plane-wave basis[S3] (E_{cut} = 50 eV) with pseudoization.[S4] The *quantum espresso v.6.5* software package[S5] and "norm-conserving" pseudopotentials from the pslib v1.0 library[S6] were used. The Effective Screening Medium Method[S7] was applied to avoid the electrostatic via-space interaction of the simulated and the “back” edge of the ribbon images. The choice of k-points and the use of spin polarization varied between the calculations. We performed a series of spin-polarized and unpolarized gamma-point calculations and a series of spin-polarized calculations with the number of k points inversely proportional to the cell size, i.e. 6 k points for the x2 cell, 4 for the x3 cell, 3 for the x4 cell, and 2 for the x6 cell. So, the product of the k-points number and the cell size along the ribbon remained constant. The k-point positions were determined automatically using the Monkhorst-Pack scheme.[S8] Figure 1 depicts the supercell for M edge model. In the calculations, molybdenum and sulfur atoms of the two bottom rows were fixed and positions of the remaining atoms were optimized. Where the “back” edge was modified with hydrogen, the position of hydrogen atoms was not fixed. The starting positions of molybdenum and sulfur atoms were selected so that the ribbon corresponded to the idealized fragment of the molybdenum disulfide crystal structure. In the M edge model, additional sulfur atoms ("edge" sulfur) were introduced into the bridge positions between molybdenum atoms. Starting polarization of some atoms was introduced in spin-polarized calculations. Sometimes different starting spin polarizations can lead to different final energies and geometry, and, if such is the case, the lower energy structure from among the resulting ones was employed. Since common optimization algorithms are inefficient if symmetry of the starting geometry is higher than the minimum,[S9, S10] several arbitrarily selected model edge atoms were shifted from the starting position by 0.3-0.5 A.

Maps of electron density and spin polarization in the plane of metal atoms were calculated for all models. Since electron density maps of different models appeared to be rather similar due to

the analogous position of atoms, post-processing was implemented to highlight the differences in electron density distribution. For this purpose, the electron density maps for x2 and x3 models were first averaged over the shifts for the period of the ribbon positioning along the edge and then between each other and, after that, the map of the difference between the electron density of a separate model cell and this electron density of comparison was built. The spin-polarization maps did not require such processing. All the maps can be found in Supporting Materials. The paper adduces examples of the most interesting of the maps.

Appendix. Representation of the wavefunction in the plane-wave basis set

Calculations in the plane-wave basis are characterized by three main numbers: the cutoff energy for basis functions E_{cut}, k-points grid, and pseudopotentials. E_{cut} defines the size of the basis. Plane-wave basis functions have form of

$$f_n(\mathbf{r}) = c_n \cdot \exp\cdot(i \cdot \mathbf{G}_n \cdot \mathbf{r}),$$

where c_n – normalization factor, $\mathbf{G}_n$ – vector in reciprocal space, $\mathbf{r}$ – radius vector in real space, and i – imaginary unit.

If to confine to periodic functions with the predetermined periodic boundary conditions, the G vector can take on only discrete values that form an infinite grid in reciprocal space. In this case, the larger the size of the subject supercell, the higher the density of the lattice in reciprocal space. The kinetic plane wave energy in atomic units is $0.5|G|^2$, and truncating the problem to include only waves for which this value is lower than E_{cut} limits the size of the basis and the frequency of the fastest oscillating wave.

One-electron wavefunctions in the plane-wave basis set are built as

$$\psi_n(\mathbf{r}) = \exp(i \cdot \mathbf{k} \cdot \mathbf{r}) \cdot u(\mathbf{r}),$$

where $u(\mathbf{r})$ – functions with the period equal to the calculated cell size; $\mathbf{k}$ – arbitrary vector in reciprocal space.

In theory, for studying the properties of an infinite crystal, it is necessary to take into account plane waves with all possible k vectors. However, based on the fact that u(r) in the used representation is also decomposed to plane waves, it may be written that

$$\psi_n(\mathbf{r}) = c_{n,\mathbf{G}+\mathbf{k}} \cdot \exp\cdot(i \cdot (\mathbf{G}+\mathbf{k}) \cdot \mathbf{r}).$$

On the right side is the summation over all possible G and k values. Since the admissible G values form a periodic grid, any vector of G + k values can be represented as G'+ k', where k' is a vector in a certain arbitrarily chosen repeated cell in reciprocal space. As a rule, for the role of such cell is selected the so-called first Brillouin zone (hereinafter 1.B.z.), i.e. a repeated reciprocal space grid element centered at the zero point (the full definition is much more sophisticated). It means that for any wave

$$\varphi(\mathbf{r})=\exp(i\cdot\mathbf{k}_\varphi\cdot\mathbf{r})\cdot u_\varphi(\mathbf{r}),$$

where k is beyond the limits of the 1.B.z, it is possible to find such $\mathbf{k}'_\varphi$ and $\mathbf{u}'_\varphi$:

$$\varphi(\mathbf{r})=\exp(i\cdot\mathbf{k}'_\varphi\cdot\mathbf{r})\cdot u'_\varphi(\mathbf{r})=\exp(i\cdot\mathbf{k}_\varphi\cdot\mathbf{r})\cdot u_\varphi(\mathbf{r}).$$

Moreover, since wavefunctions with close k are similar, calculations can include the finite number of trial vectors of k - k *points*. In this case, the larger the real-space cell volume, the smaller the reciprocal space cell volume and, accordingly, the fewer k-points are needed for calculations with acceptable accuracy. If the original cell has symmetry elements, this generates symmetry in the 1.B.z., which allows reducing the number of unique k-points that have to be calculated.

An independent calculation of wavefunctions is performed for each k-point. The observed integral crystal characteristics are the averaging of the result over all k-points. The difference in the calculation with increased k-point numbers is usually not very large, especially for large supercells, so a small number of k-points is sufficient for simple chemical modeling. However, to describe the one-electron properties (spectroscopy, structure of electronic bands, conductivity, etc.) of a real crystal, the required number of k-points can be quite large, especially in the case of crystals with a small cell.

In substance, taking several k-points in a certain direction means that we allow electron waves in that direction to have several different lengths, of which at least some are incompatible with the cell size. This is necessary if the calculation in this direction is infinitely periodic. If the periodicity in this direction is not needed (for example, it crosses the vacuum gap that simulates the crystal boundary), it is reasonable to use only one k-point. In case the supercell in real space along the x-axis is twice enlarged, the reciprocal space cell size in this direction is halved, i.e. to ensure the same density of the grid of k-points, their number should be twice less. Alternatively: taking the k-point with the $x = 0.5\ G_x$ coordinate means that the wave has the two-cell period in this direction. So, taking two k-points with $0.5\ G_x$ and $1.0\ G_x$ coordinates is equivalent to cell doubling in the x direction, where in the "image" the atomic coordinates and overall electron density distribution

repeat those of the actual subject cell. If the supercell is large enough and it is not required to boost the infinite periodicity in any direction, one can confine to one k-point in the entire calculation. If selected in a special manner (the so-called gamma point), it will reduce the calculations by about half.

The last crucial parameter is a choice of pseudopotentials. Pseudopotentials play a dual role: firstly, they allow to ignore core electrons in the calculation (it is achieved by the same means as in using the GTO basis set) and, secondly, they facilitate a description of the electron behavior near nuclei. Electron wavefunctions near the nuclei have especially strong gradients and various correction schemes are used to avoid using the extremely high E_{cut}. As in the case of atomic bases in the GTO basis sets, the corrections are selected separately for each element. Each pseudopotential for the plane- wave basis requires its own minimum E_{cut}.

When calculating systems with nonzero total spin and open systems in general, two families of spin-polarized waves with oppositely directed spins are considered in the plane-wave basis. There are various schemes for accounting for macroscopic magnetization. In this study, magnetization in the case of spin-polarized models was assumed as directed along the z axis in the model ribbon plane.

References

S1 N. Argaman and G. Makov, *Am. J. Phys.,* 2000*,* **68,** 69.

S2 J.P. Perdew, K. Burke and M. Ernzerhof, *Phys. Rev. Lett*., 1996, **77,** 3865.

S3 E.J. Bylaska, *Comput. Chem.*, 2017, 185–228.

S4 D.R. Hamann, M. Schlüter and C. Chiang, *Phys. Rev. Lett*., 1979, **43,** 1494.

S5 P. Giannozzi, O. Baseggio, P. Bonfà, D. Brunato, R. Car, I. Carnimeo, C. Cavazzoni, S. de Gironcoli, P. Delugas, F. Ferrari Ruffino, A. Ferretti, N. Marzari, I. Timrov, A. Urru and S. Baroni, *J. Chem. Phys*., 2020, **152,** 154105.

S6 A. Dal Corso, *Comput. Mater. Sci*., 2014, **95,** 337.

S7 M. Otani and O. Sugino, *Phys. Rev. B*., 2006, **73,** 115407.

S8 A. Primo, J. He, B. Jurca, B. Cojocaru, C. Bucur, V.I. Parvulescu and H. Garcia, *Appl. Catal. B Environ*., 2019, **245,** 351.

S9 H.B. Schlegel, *Adv. Ser. Phys. Chem.*, 1995, 459.

S10 J.A. Spirko, M.L. Neiman, A.M. Oelker and K. Klier, *Surf. Sci*., 2003, **542,** 192.

Maps group

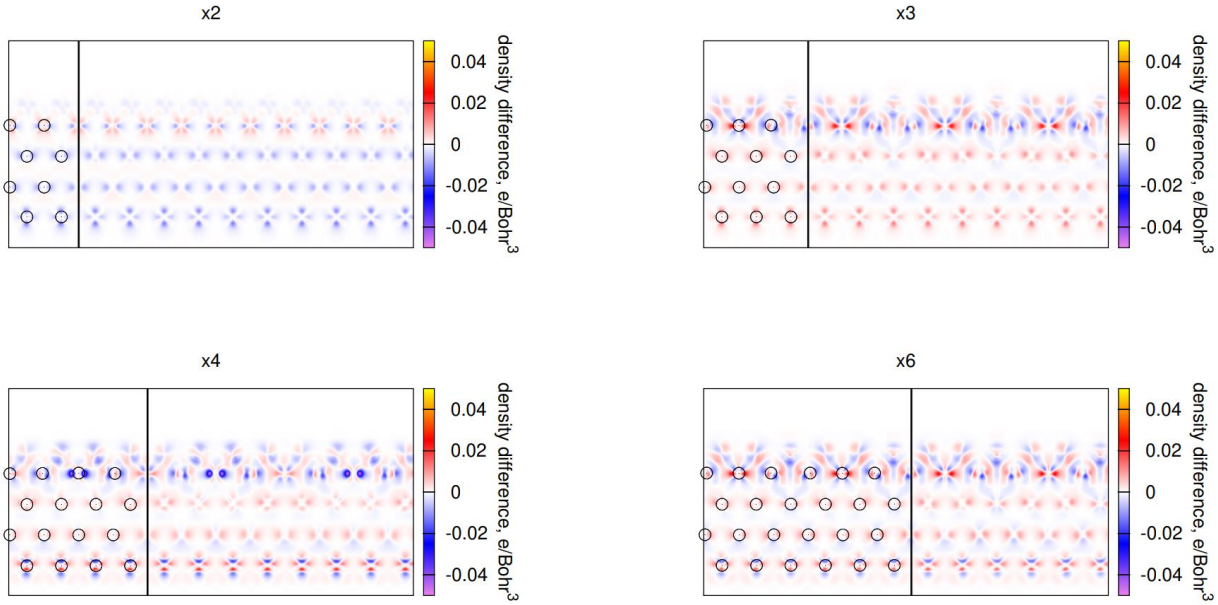

Figure S1. Maps of difference of electron density of a model with averaged electron density of models x2 and x3 (averaged over shifts by crystal structure period) for common model of M-edge without spin-polarization with gamma-point.

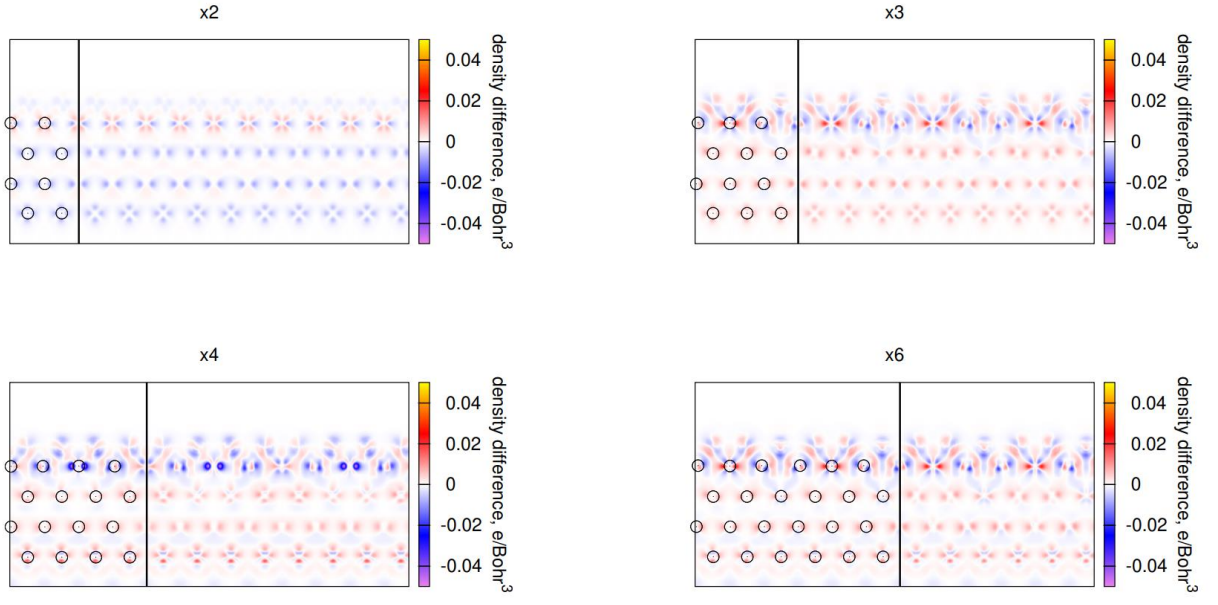

Figure S2. Maps of difference of electron density of a model with averaged electron density of models x2 and x3 (averaged over shifts by crystal structure period) for model of M-edge without spin-polarization with gamma-point with back S-edge modified by hydrogen.

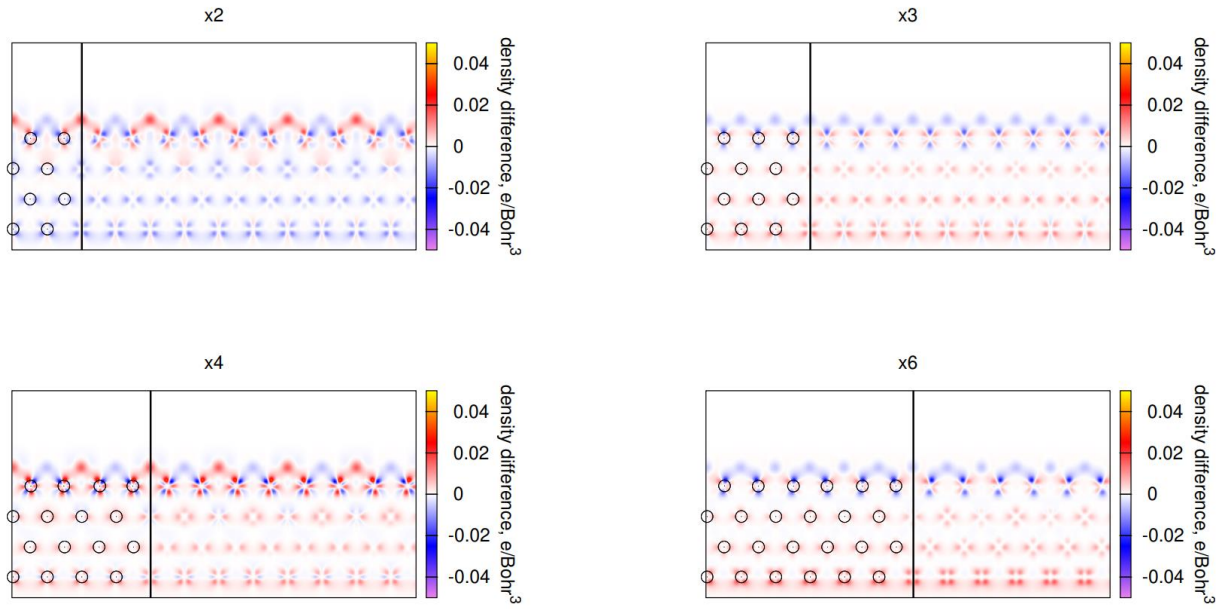

Figure S3. Maps of difference of electron density of a model with averaged electron density of models x2 and x3 (averaged over shifts by crystal structure period) for common model of S-edge without spin-polarization with gamma-point.

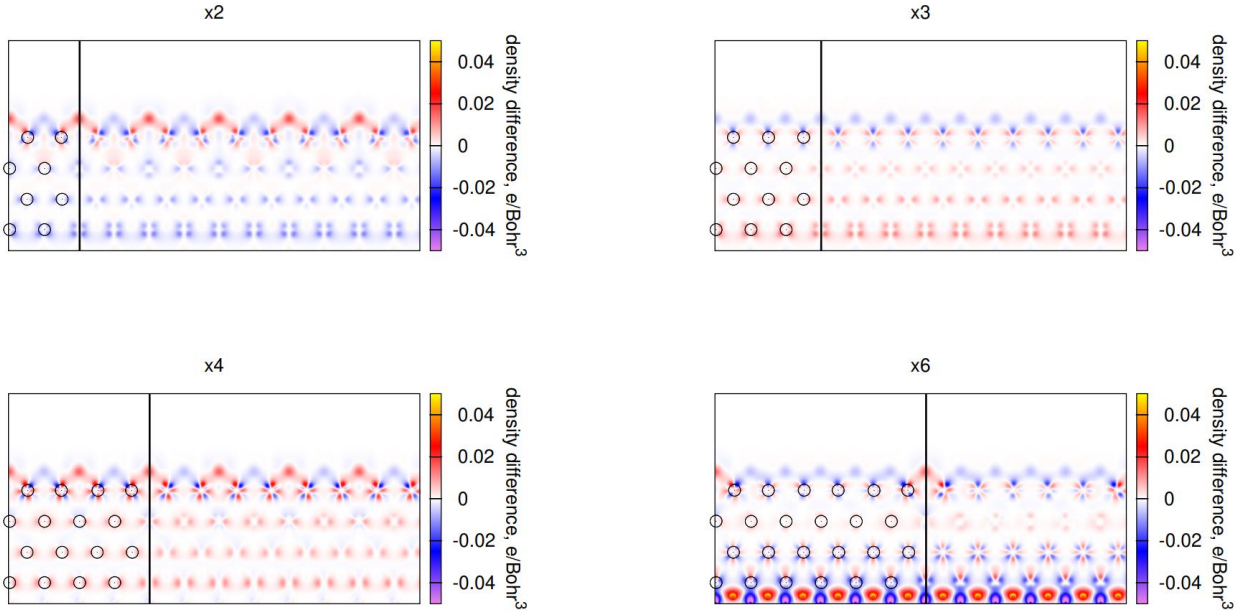

Figure S4. Maps of difference of electron density of a model with averaged electron density of models x2 and x3 (averaged over shifts by crystal structure period) for model of S-edge without spin-polarization with gamma-point with back M-edge modified by hydrogen.

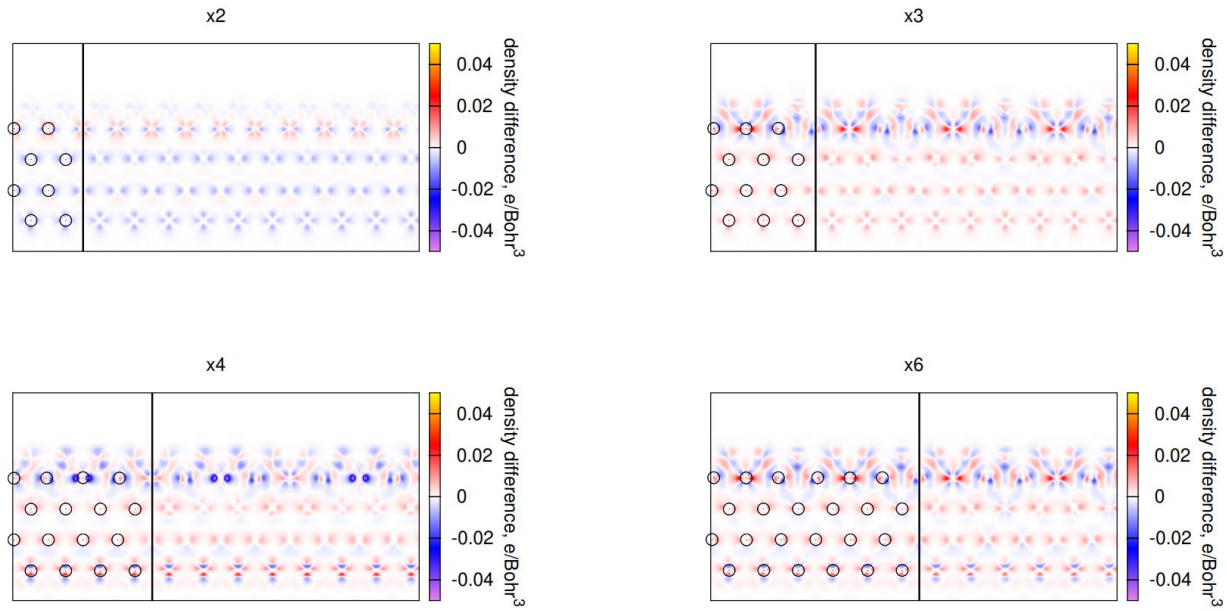

Figure S5. Maps of difference of electron density of a model with averaged electron density of models x2 and x3 (averaged over shifts by crystal structure period) for common model of M-edge with spin-polarization with gamma-point.

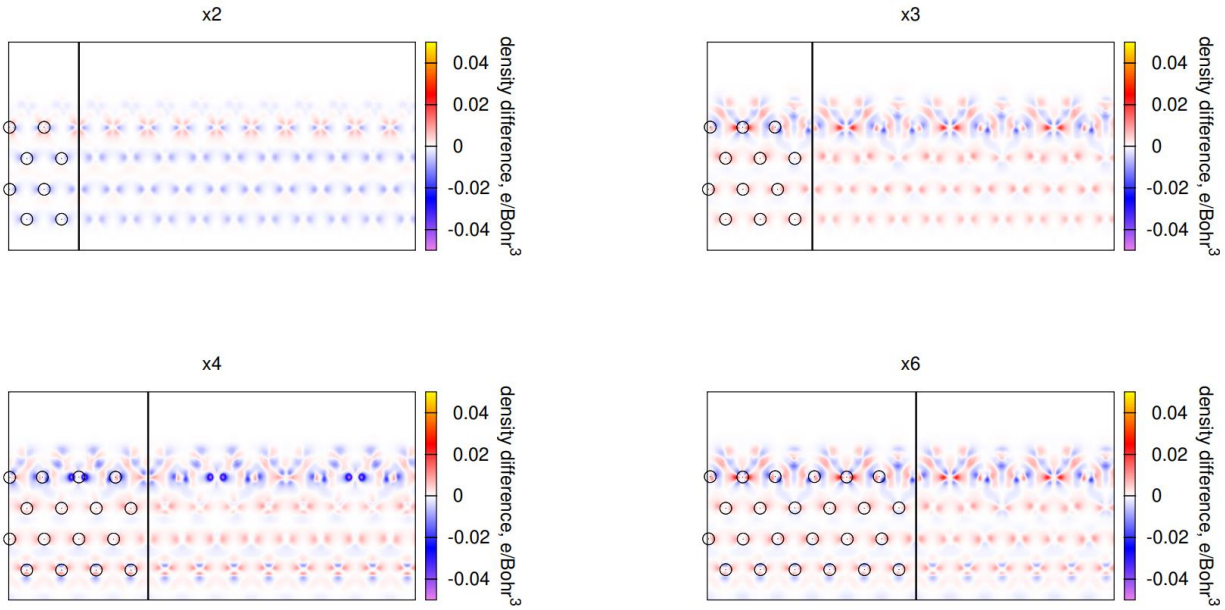

Figure S6. Maps of difference of electron density of a model with averaged electron density of models x2 and x3 (averaged over shifts by crystal structure period) for model of M-edge with spin-polarization with gamma-point with back S-edge modified by hydrogen.

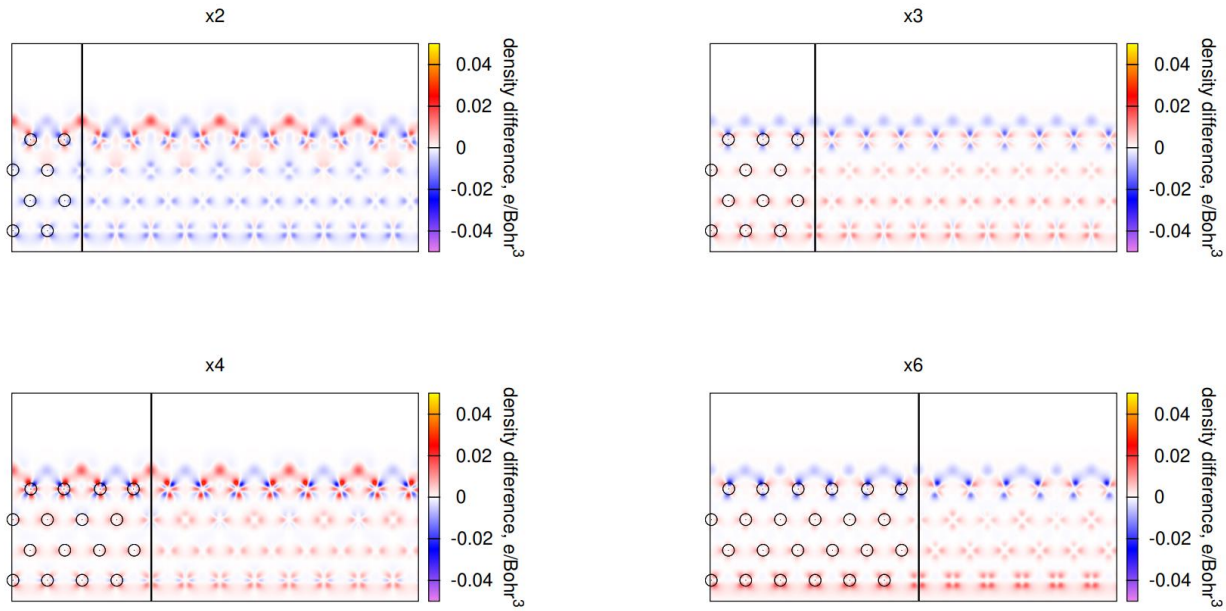

Figure S7. Maps of difference of electron density of a model with averaged electron density of models x2 and x3 (averaged over shifts by crystal structure period) for common model of S-edge with spin-polarization with gamma-point.

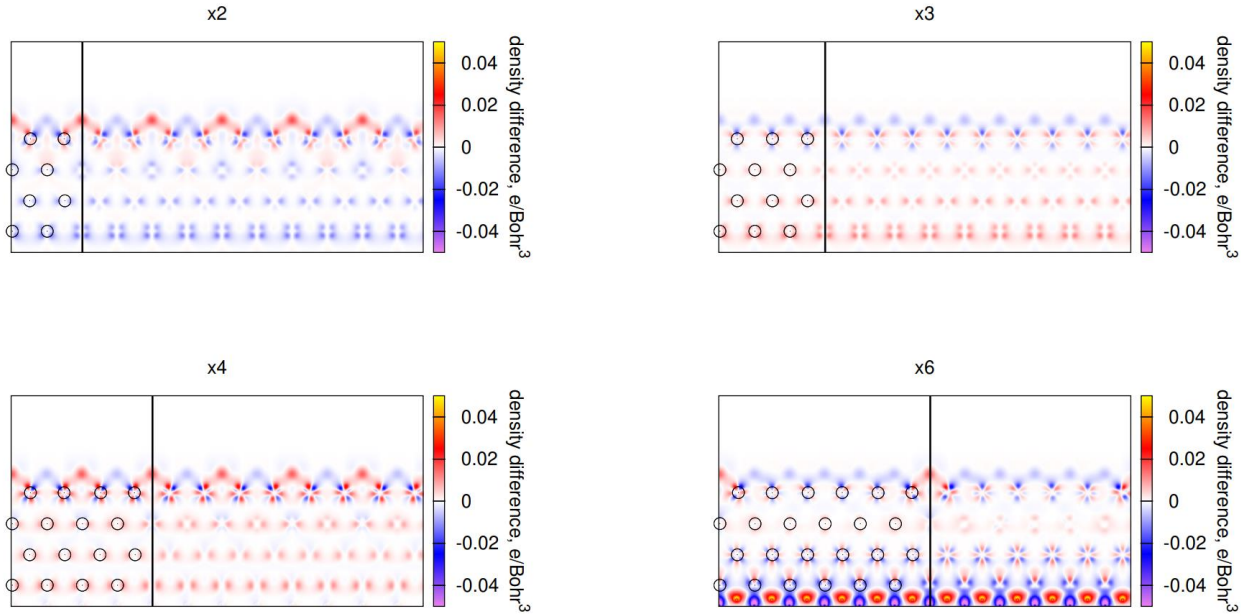

Figure S8. Maps of difference of electron density of a model with averaged electron density of models x2 and x3 (averaged over shifts by crystal structure period) for model of S-edge with spin-polarization with gamma-point with back M-edge modified by hydrogen.

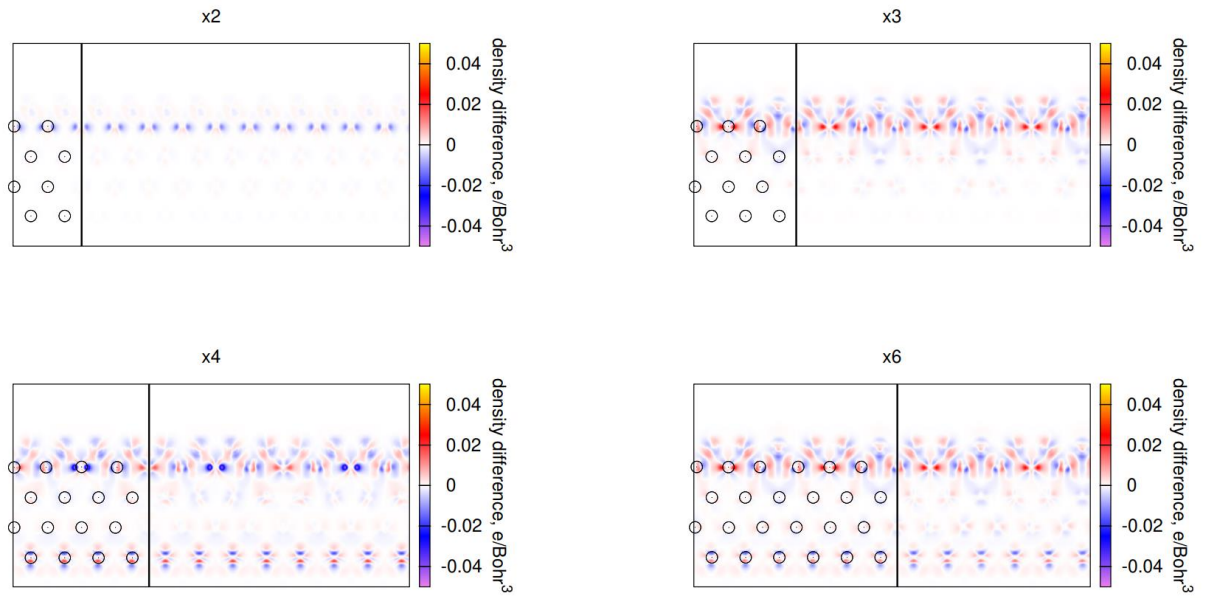

Figure S9. Maps of difference of electron density of a model with averaged electron density of models x2 and x3 (averaged over shifts by crystal structure period) for common model of M-edge with spin-polarization with varying number of k-points.

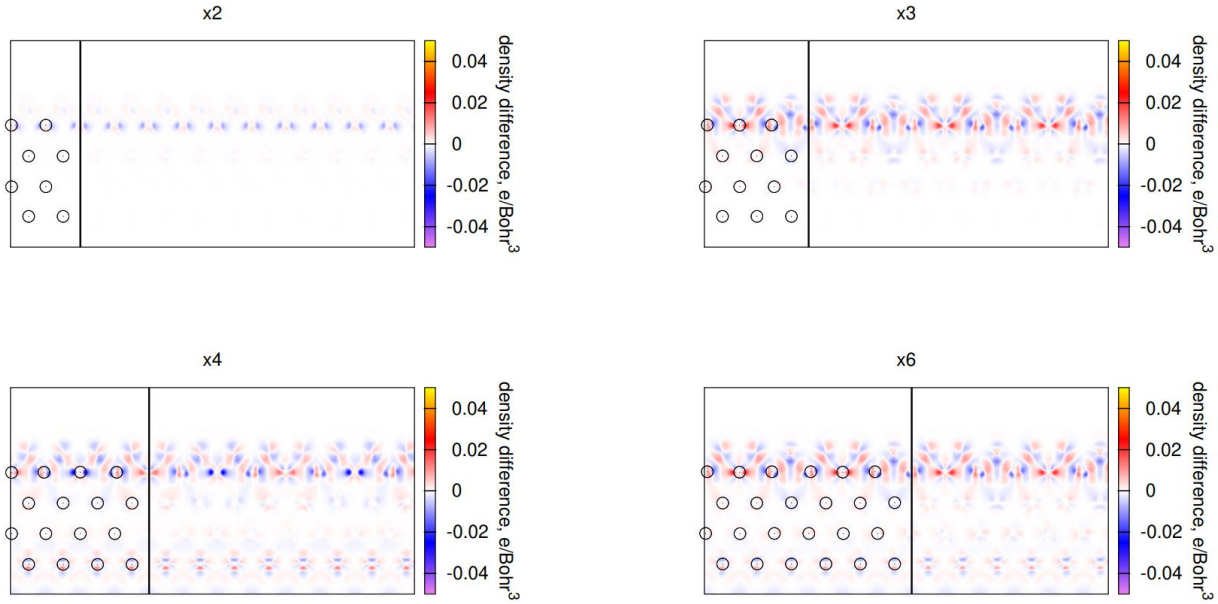

Figure S10. Maps of difference of electron density of a model with averaged electron density of models x2 and x3 (averaged over shifts by crystal structure period) for model of M-edge with spin-polarization with varying number of k-points with back S-edge modified by hydrogen.

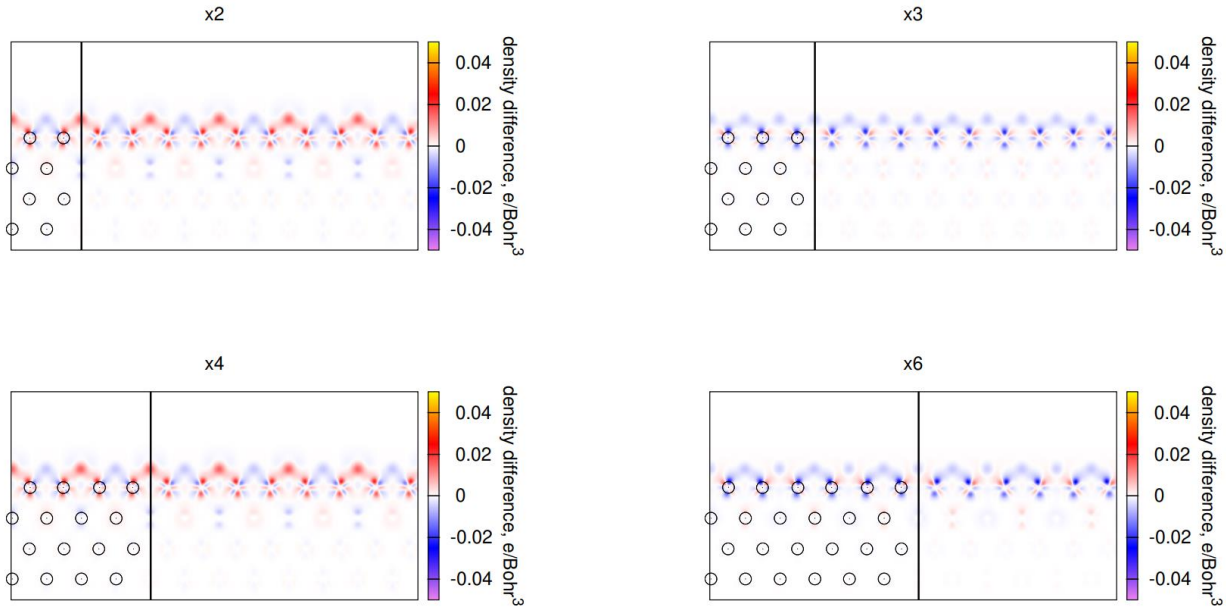

Figure S11. Maps of difference of electron density of a model with averaged electron density of models x2 and x3 (averaged over shifts by crystal structure period) for common model of S-edge with spin-polarization with varying number of k-points.

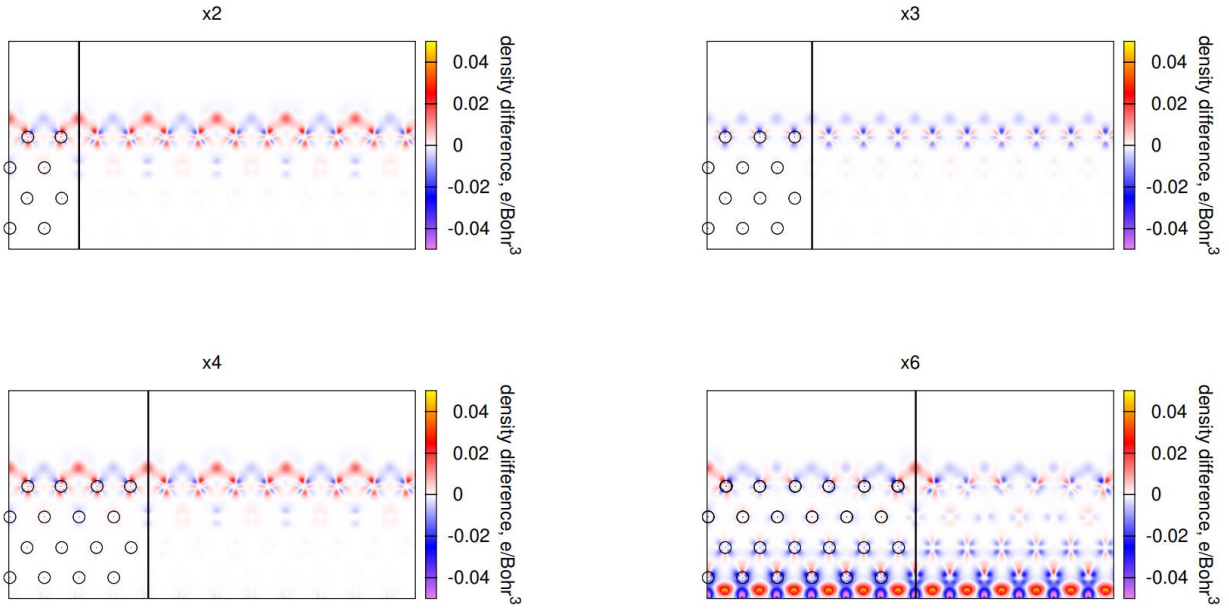

Figure S12. Maps of difference of electron density of a model with averaged electron density of models x2 and x3 (averaged over shifts by crystal structure period) for model of S-edge with spin-polarization with varying number of k-points with back M-edge modified by hydrogen.

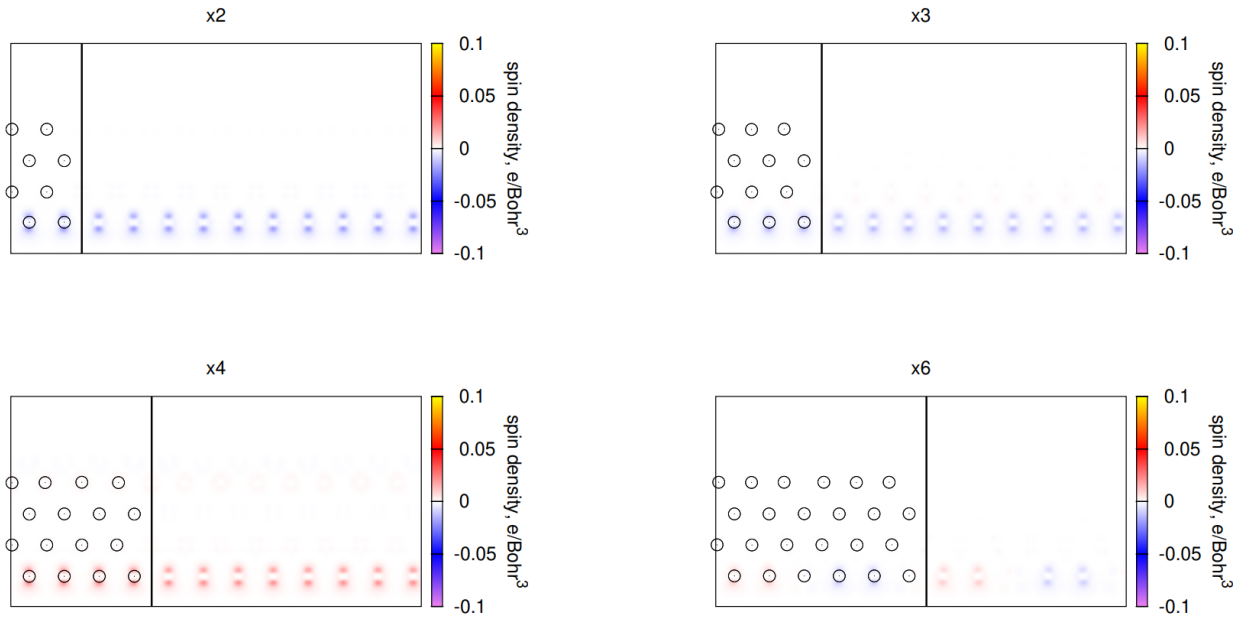

Figure S13. Maps of spin-density of a model for common model of M-edge with spin-polarization with gamma-point.

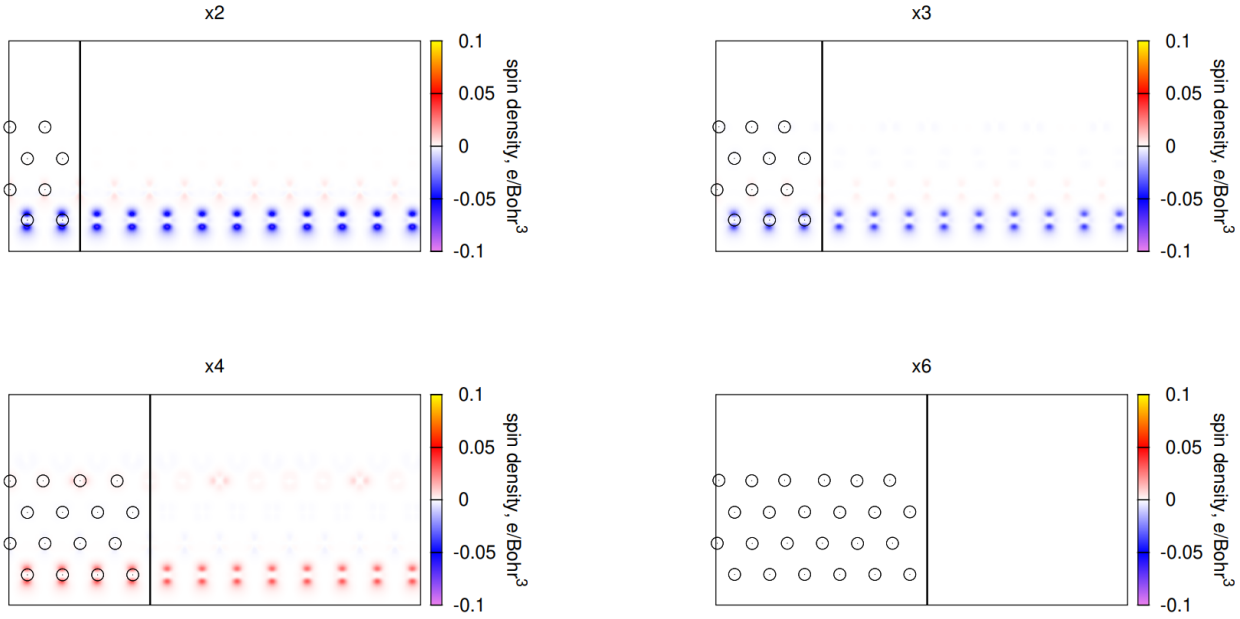

Figure S14. Maps of spin-density of a model for model of M-edge with spin-polarization with gamma-point with back S-edge modified by hydrogen.

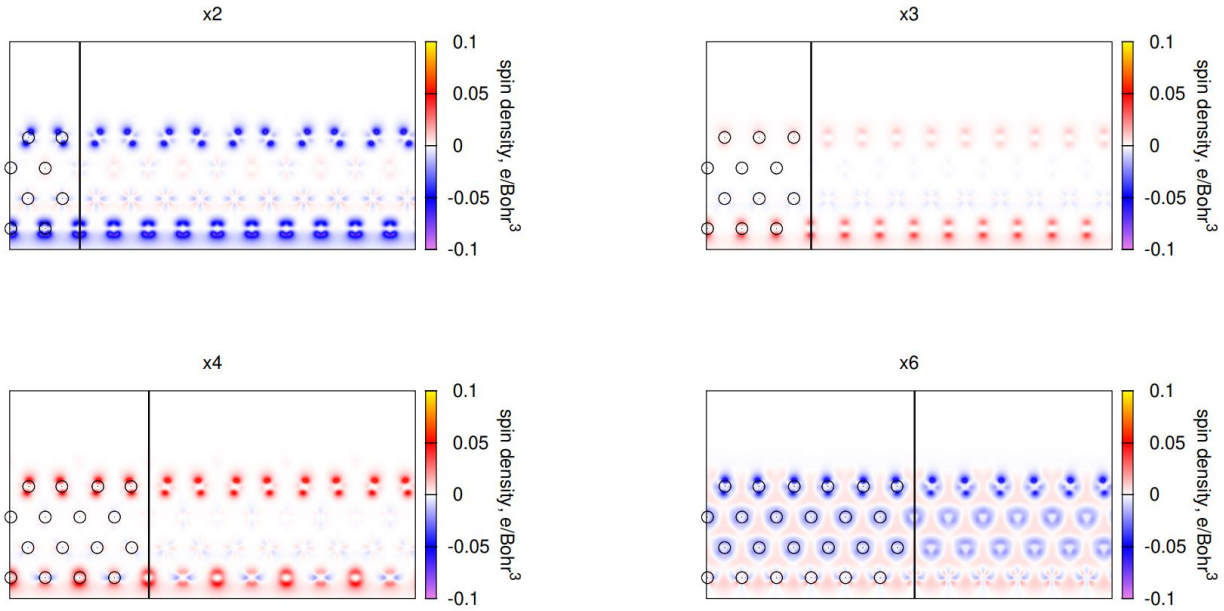

Figure S15. Maps of spin-density of a model for common model of S-edge with spin-polarization with gamma-point.

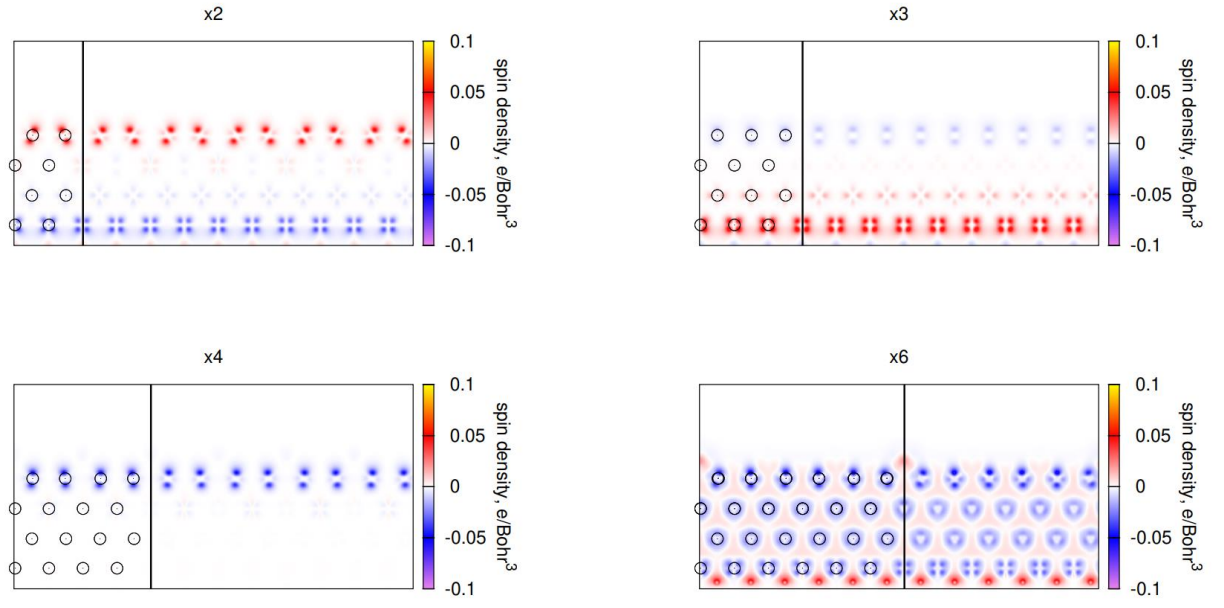

Figure S16. Maps of spin-density of a model for model of S-edge with spin-polarization with gamma-point with back M-edge modified by hydrogen.

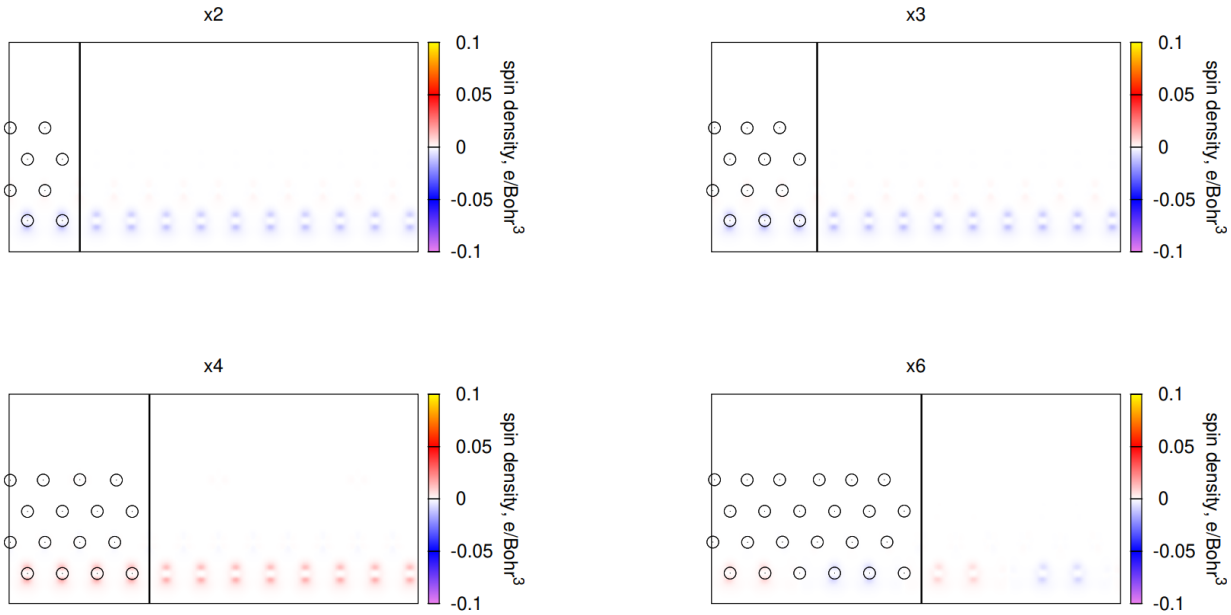

Figure S17. Maps of spin-density of a model for common model of M-edge with spin-polarization with varying number of k-points.

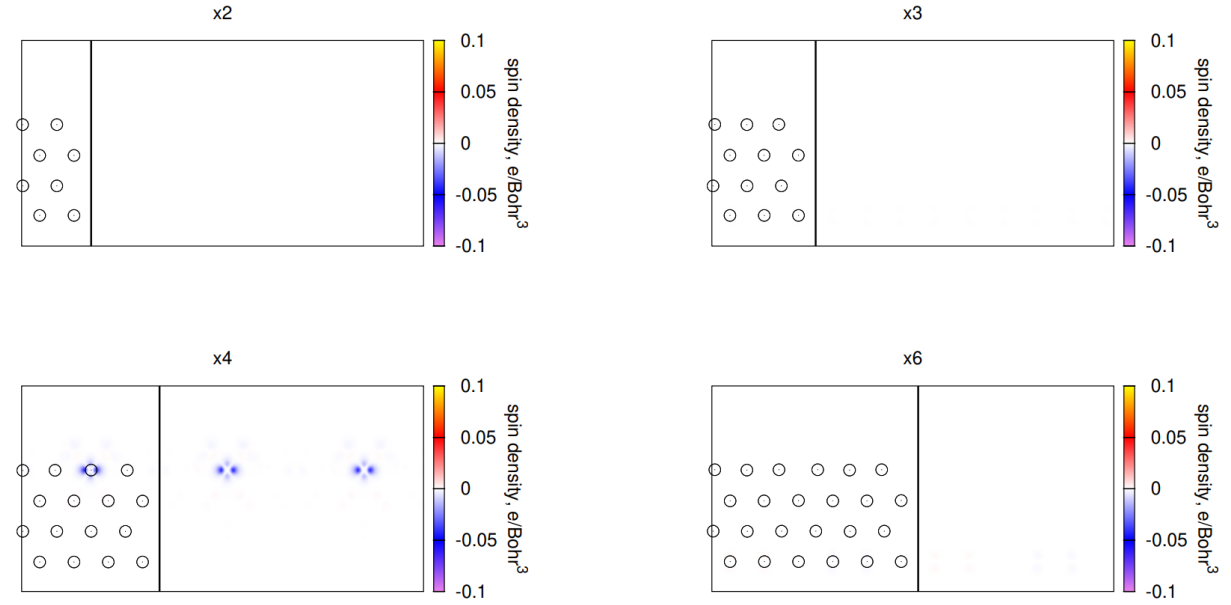

Figure S18. Maps of spin-density of a model for model of M-edge with spin-polarization with varying number of k-points with back S-edge modified by hydrogen.

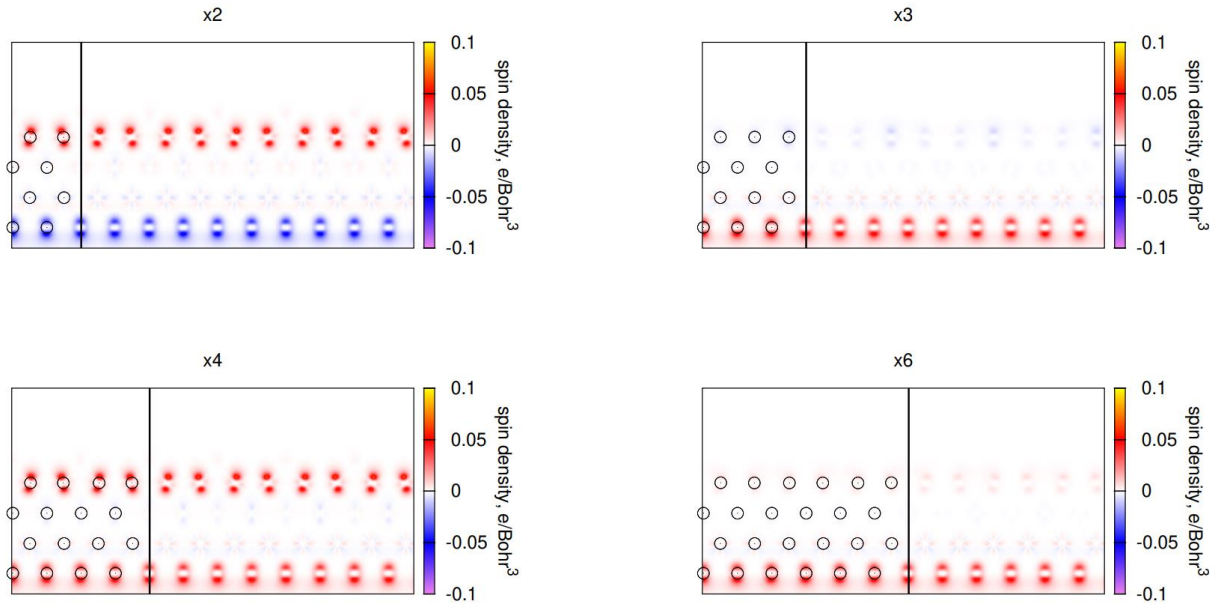

Figure S19. Maps of spin-density of a model for common model of S-edge with spin-polarization with varying number of k-points.

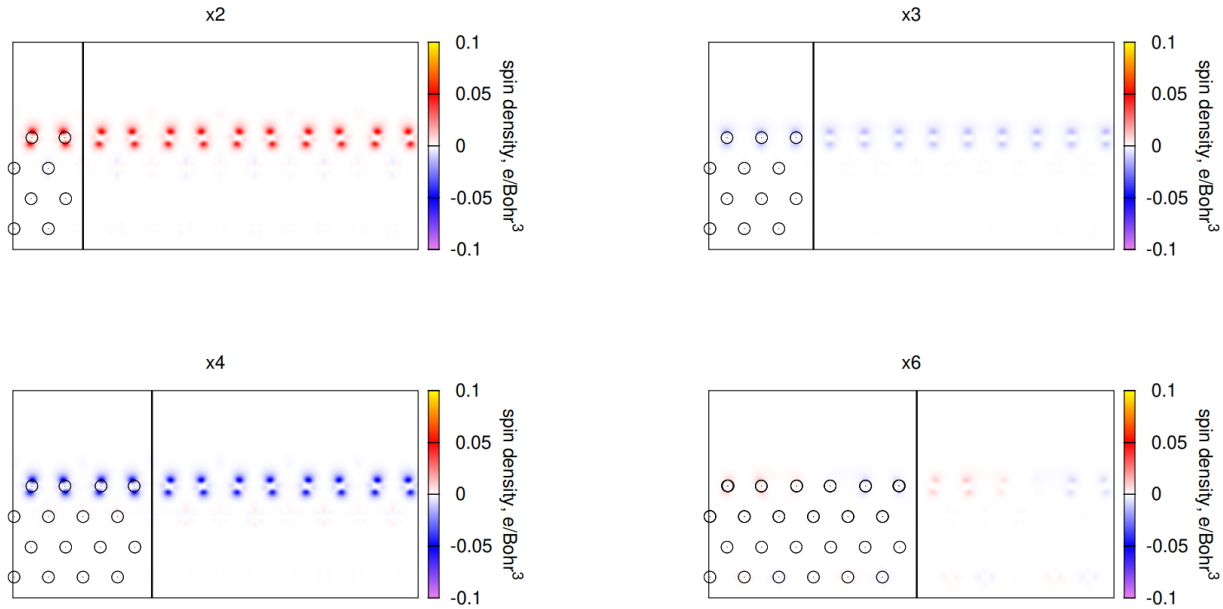

Figure S20. Maps of spin-density of a model for model of S-edge with spin-polarization with varying number of k-points with back M-edge modified by hydrogen.